Proc. Lunar Planet. Sci. Conf. 10th (1979), p. 2741–2756.
Printed in the United States of America

Calculational investigation of impact cratering dynamics: Early time material motions

Jeffrey M. Thomsen, Michael G. Austin, and Stephen F. Ruhl

Physics International Company, 2700 Merced Street, San Leandro, California 94577

Peter H. Schultz

The Lunar and Planetary Institute, 3303 NASA Road 1, Houston, Texas 77058

Dennis L. Orphal

California Research and Technology, Incorporated, 4049 First Street, Suite 135, Livermore, California 94550

Abstract—Early time two-dimensional finite difference calculations of laboratory-scale hypervelocity (6 km/sec) impact of 0.3 g spherical 2024 aluminum projectiles into homogeneous plasticene clay targets were performed and the resulting material motions analyzed. Results show that the initial jetting of vaporized target material is qualitatively similar to experimental observation. The velocity flow field developed within the target is shown to have features quite similar to those found in calculations of near-surface explosion cratering. Specific application of Maxwell's analytic Z-Model (developed to interpret the flow fields of near-surface explosion cratering calculations), shows that this model can be used to describe the flow fields resulting from the impact cratering calculations, provided that the flow field center is located beneath the target surface, and that application of the model is made late enough in time that most of the projectile momentum has been dissipated.

INTRODUCTION

Calculations can facilitate understanding of the dynamics of cratering processes which have been studied in detail in laboratory-scale impact experiments (Gault *et al.*, 1968; Oberbeck, 1971; Gault and Wedekind, 1977; Moore, 1976). Relatively few impact calculations have been performed, and fewer still have directly addressed impacts at scales for which experimental and theoretical results can be compared. Bjork (1961) and Bryan *et al.* (1978) calculated a terrestrial impact crater, Meteor Crater in Arizona. O'Keefe and Ahrens (1975) emphasized the early-time shock effects of a large meteorite impact at 15 km/sec into a material thought to be typical of the early lunar crust. Similar calculations of small-scale impact (O'Keefe and Ahrens, 1978) examined scaling of the above results and, through ballistic extrapolation, the ejecta distribution assuming lunar gravity (O'Keefe and Ahrens, 1976). O'Keefe and Ahrens (1977) also showed the de-

pendence of the early-time partitioning of energy on impact velocity in the range of 5 to 45 km/sec.

The present calculational effort examines the fundamental impact dynamics in a uniform, non-geologic material at impact velocities achievable in laboratory-scale experiments. Impact shock effects in the target and the resultant initial material motions are computed and examined during the *compression stage* and the early part of the *excavation stage* of laboratory-scale impact crater formation, as described empirically by Gault *et al.* (1968). The *compression stage* described the events associated with the initial contact between the projectile and the target. This included the shock compression of the target material directly below the projectile and the subsequent hydrodynamic motion of that material. This stage was defined to terminate at approximately the time of complete engulfment of the projectile by the target. The *excavation stage* then begins. It described the basic shock wave geometry generated in the target and the resulting motions of the target material. It was empirically observed that the initial dominantly radial motions (centered close to the point of impact) were subsequently modified by a continuous fan of rarefaction waves originating at the target surface. These waves caused an upward velocity component to develop in the shocked target material which led eventually to the orderly ejection of target material from the impact area. The end result of the *excavation stage* was a bowl-shaped depression; this is also known as the final stage of development of the transient crater.

During the *compression stage* the present effort discusses the dynamics of the initial contact between the projectile and the target from a calculational viewpoint. Energy and momentum transfer from the projectile to the target (quantities not directly observable in impact experiments) are discussed, as are the processes of shock heating and vaporization. The latter are relevant because of the specific target and projectile materials chosen. Only the initial radial motions during the *excavation stage* of Gault *et al.* (1968) are examined. An analytic model developed by Maxwell (1977) to describe the explosive cratering excavation process is applied to the impact cratering calculations. This model, the Z-Model, implies an orderly ejection of material from the cratering region in a manner very similar to that observed empirically by Gault *et al.* (1968).

INITIAL CONDITIONS, MATERIALS, AND MATERIAL MODELS

Figure 1 summarizes the initial conditions for the calculations. The calculations simulate the impact of 6 mm diameter 2024 aluminum projectiles into plasticene (oil base) clay targets. Axial symmetry and terrestrial gravity are assumed. It is also assumed that the impacts occur in a vacuum chamber. Two calculations were performed in which only the clay strength was varied.

The present effort is directed toward a better understanding of cratering dynamics, and not toward simulation of a specific planetary impact event. For this purpose plasticene clay has properties which make it rather unique as a target material. It has a simple equation of state description, primarily because it con-

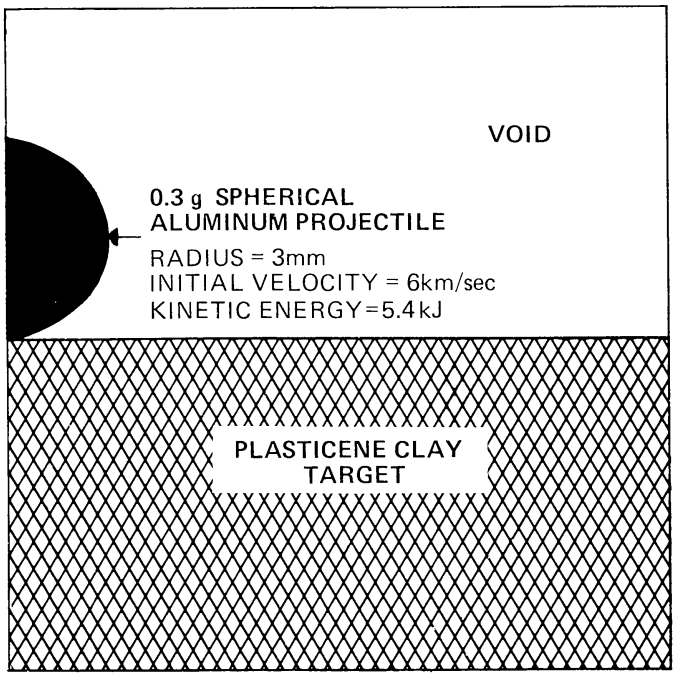

Fig. 1. Summary of calculation initial conditions.

tains no air voids. Its shear strength can also be simply characterized by a von Mises (Maxwell and Reaugh, 1972) or Mohr-Coulomb (Holsapple and Schmidt, 1979) criterion, and the strength magnitude can be changed by varying the ambient temperature. Finally, it is readily available, and this should allow close integration of this calculational effort with future experimental studies.

Static material properties determined for plasticene clay (Christensen *et al.*, 1968) are: an initial density of 1.69 Mg/m^3, a compressional wave velocity of 1.4 m/msec, a shear wave velocity of 0.475 m/msec, and a Poisson's ratio of 0.435.

The equation of state for plasticene clay (Maxwell and Reaugh, 1972) is based on Hugoniot data from Christensen *et al.* (1968) presented in Table 1. From these data the relative volumes and internal energies were calculated using Hugoniot relationships (see for example McQueen *et al.*, 1970). The equation of state form which matches these states gives the pressure P(GPa), as a function of compression, V [where $V = \rho_0 \div \rho$; $\rho_0(Mg/m^3)$ is the initial density and $\rho(Mg/m^3)$ is

Table 1. Plasticene Hugoniot data from Christensen *et al.* (1968).

Measured shock velocity U_s (km/sec)	Calculated particle velocity U_p (km/sec)	Measured pressure P(GPa)
3.7	0.91	5.75
5.6	2.26	21.4*

*Represents the average of two measurements.

the current density]; compressibility, μ [where $\mu = (1 - V) \div V$]; and energy density, E(GJ/m^3):

$$\begin{aligned} P &= 2.8\,\mu + 40.7\,\mu^2 - 36.0\,\mu^3 + 1.7\,E/V \qquad \mu \geq 0 \\ P &= 1.7\,E/V \qquad \mu < 0. \end{aligned} \tag{1}$$

This form incorporates the initial (zero pressure) bulk modulus of 2.8 GPa, provides the required fit to the Hugoniot data, and allows for reasonable extrapolation to pressures greater than those covered by experimental data ($0 \leq P \leq 21.4$ GPa).

A von Mises failure envelope was used in the calculations reported here; the actual von Mises strength was found to be dependent on the ambient clay temperature, T (Maxwell *et al.*, 1972), so two calculations with differing strengths were performed. One calculation used the estimated low strength (50 kPa, T = 32.2°C) and the other used a higher strength (150 kPa). We did not expect the results of the two calculations to differ greatly during the compression stage or the early part of the excavation stage discussed here, when the impact-induced shock pressures greatly exceeded the clay strengths. Explosive cratering experiments in plasticene clay (Maxwell *et al.*, 1972) revealed, however, that the final crater volume increased by a factor of three as the ambient clay temperature increased from 17.5 to 32.2°C. Thus, when we examine (in the future) the calculational results near the end of the excavation stage, we expect significant differences to appear.

The equation of state for 2024 aluminum was a Hugoniot fit reported by van Thiel (1977) based on the Hugoniot measurements of McQueen *et al.* (1970):

$$P(\text{GPa}) = \frac{\rho_0 C_0^2 \mu\,(1 + \mu)}{[1 + \mu\,(1 - s)]^2} \qquad 8.4 \leq P \leq 109\ \text{GPa}, \tag{2}$$

where $\rho_0 = 2.783$ Mg/m^3; C_0 (the bulk sound speed) = 5.343 m/msec and s = 1.325. The maximum strength of the aluminum Mohr-Coulomb failure envelope used [320 MPa, van Thiel (1977)] is much greater than the clay strengths.

The one-dimensional pressure state generated behind the shock during the impact of the aluminum sphere into the plasticene clay target at 6 km/sec was determined from Equations 1 and 2 using the method of Gault and Heitowit (1963). The calculated pressure of 50 GPa (Fig. 2) is not sufficient to shock melt aluminum, as a shock pressure of 60 GPa is required to cause incipient melting (Gehring, 1970). Maxwell and Reaugh (1972) estimated that incipient vaporization of the volatile constituents of the plasticene clay begins at a pressure of about 6 GPa. This latter pressure is substantially lower than 50 GPa, indicating that vaporization of the clay target will occur during the compression stage.

CALCULATIONAL PROCESS AND RESULTS OF INITIAL IMPACT

Figure 3 shows vector velocities in the target material during the compression stage and also illustrates the initial part of the calculational process. The two-

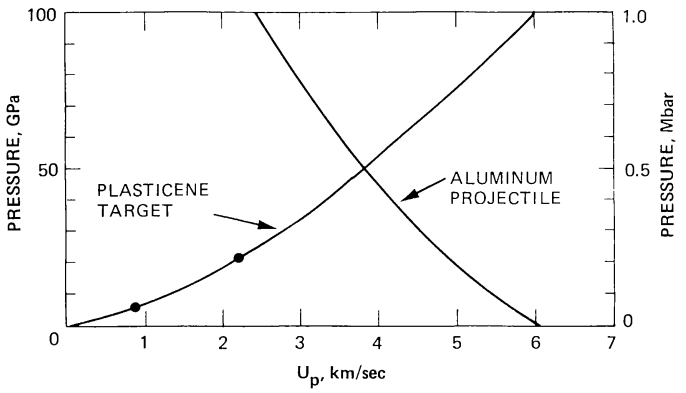

Fig. 2. Intersection of curves defining the one-dimensional theoretical pressure state occurring behind the shock front for an aluminum projectile with a velocity of 6 km/sec impacting into a plasticene clay target. The two clay experimental data points of Christensen *et al.* (1968) are also shown.

dimensional computer code used, PISCES 2D ELK (Hancock, 1976), permitted initial modeling of the projectile using a Lagrangian finite difference approximation and the target using an Eulerian approximation. As the projectile moved into the target, it interacted continuously along its outer boundary with the target. In the computer code treatment the Lagrangian grid literally "moves through" the Eulerian grid. Material cannot occupy simultaneously the same point in space in both grids, however, and the Lagrangian material predominates. Thus the Eulerian target material gets pushed out of the way by the impacting Lagrangian projectile; momentum and energy are transferred continuously, and a shock wave is formed in the target. The Lagrangian projectile zone size is shown explicitly. The zone size in the Eulerian target region was initially 0.3 mm square, and thereby spanned the initial projectile radius with ten radial zones.

A maximum pressure of 42.1 GPa was observed in the calculations at the earliest time when the Eulerian cell variables were printed out after the initial impact (0.155 μsec). It occurred close to the symmetry axis directly below the projectile. The target region spanning the projectile contact radius was all highly compressed, and a shock wave was quickly formed in the clay. By 0.3 μsec (Fig. 3a), the presence of the free surface beyond the projectile contact radius caused rarefaction waves to relieve the shock pressures in the clay at the point of projectile contact with the original target surface; but in doing so a jet of vaporized clay was formed. The vector velocities of Fig. 3 above the target surface depict the magnitude and direction of the jet. The maximum jet velocities (10.0 km/sec) occurred in the lowest density jetted material ($1–2 \times 10^{-6}$ Mg/m^3), but that with the highest specific internal energy. The density cutoff value in each Eulerian cell was 10^{-6} Mg/m^3; lowering the cutoff value to 10^{-7} Mg/m^3 resulted in a maximum jet velocity of 10.7 km/sec, or only about 7 percent greater. The density associated with this slightly faster velocity was $2–3 \times 10^{-7}$ Mg/m^3.

At times up to 1 μsec (Fig. 3c) the density of the jetted material increased in the direction of the target surface. At heights of 1 mm above the surface, the

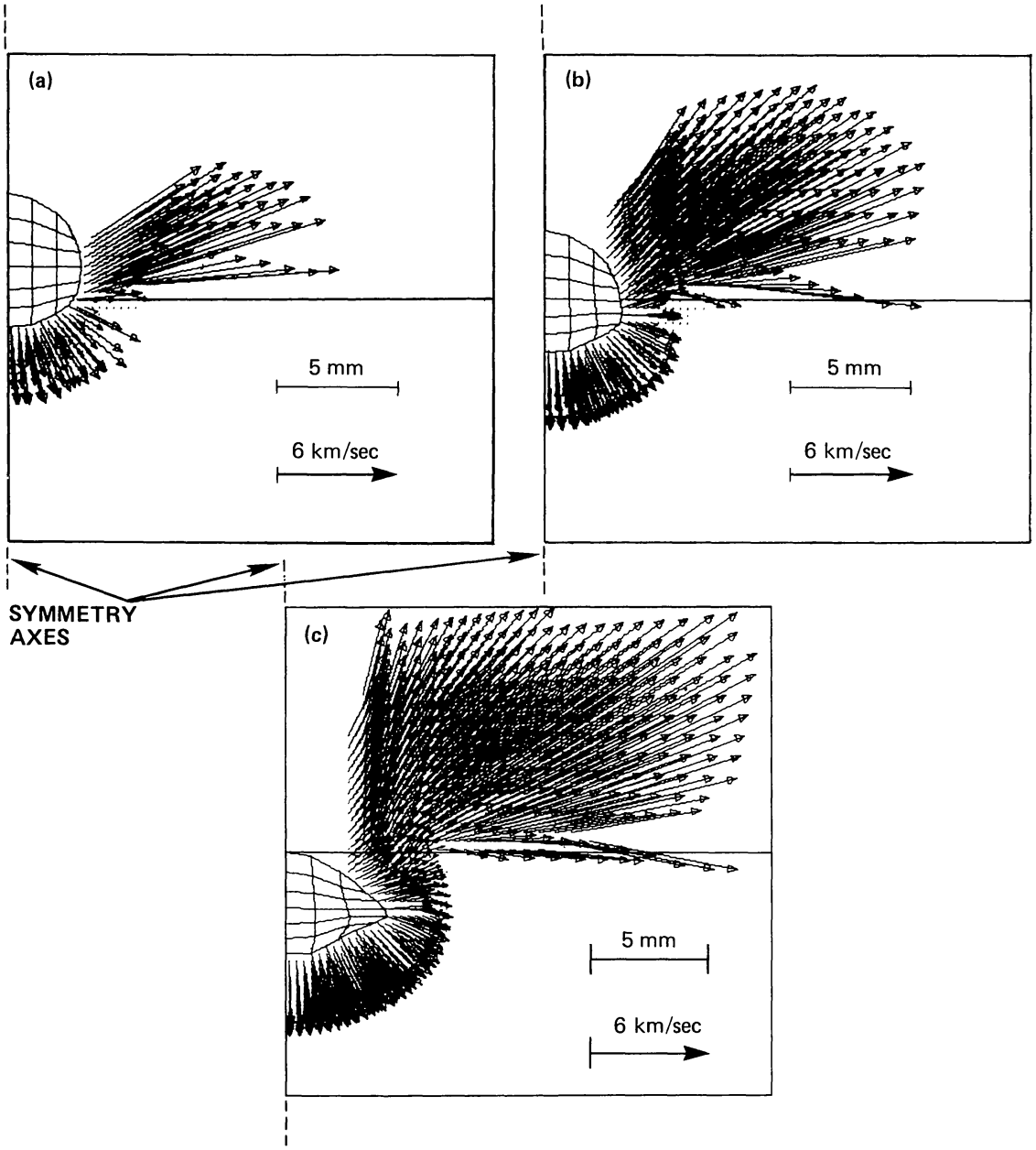

Fig. 3. Lagrangian grid of the aluminum projectile and vector velocity plots in the Eulerian grid containing the plasticene clay target, depicting the early time jetting of target material and projectile deformation at (a) 0.30 μsec, (b) 0.55 μsec, and (c) 1.02 μsec. The horizontal line through the center of each frame shows the pre-impact location of the target surface.

jetted material had a density of approximately 1 Mg/m^3, and a velocity an order of magnitude less than the maximum jet velocity. This relatively stationary material was in the form of a "lip" which controlled the direction of subsequently vaporized and jetted clay. The effect of the control is seen most clearly in Fig. 3c, where velocity vectors beyond the lip position are actually pointed in the

direction of the target surface. It is also clear from Fig. 3c that by the time of complete engulfment of the projectile by the target (approximately the end of the compression stage) the projectile had been severely deformed.

Gault *et al.* (1968) similarly described the onset of target material jetting early in the compression stage, as observed in laboratory-scale impacts into metals and natural materials. They noted that jetting velocities which are higher than the original impact velocity were also predicted by theory. The maximum calculated jetting velocities in the present effort (10.7 km/sec, or 1.8 times the original impact velocity) were in qualitative agreement with their observations. Due to materials differences, however, an exact comparison of the magnitude of their theoretically predicted jetting velocities with the calculationally derived velocities could not be made.

Vaporization of target material in the region near the impact continued to a time of about 1.5 μsec, when the shock pressures induced in the target fell to below 6 GPa. It was determined that a mass of approximately 2.75 g of target material (over nine times the projectile mass) was vaporized and that this mass contained about 1.5 kJ of internal energy (roughly 28 percent of the total impact energy). This mass of vaporized target material is very much greater than those reported by O'Keefe and Ahrens (1977) for gabbroic anorthosite or iron projectiles impacting gabbroic anorthosite targets at 7.5 km/sec. This is because both iron and gabbroic anorthosite require higher shock vaporization pressure levels than can be generated by an impact at 7.5 km/sec. The vaporized target masses in our calculations are comparable to the vaporized target masses of O'Keefe and Ahrens (1977) for gabbroic anorthosite impacting gabbroic anorthosite at 30 to 45 km/sec and for iron impacting gabbroic anorthosite at 15 to 30 km/sec.

By 2.6 μsec after initial contact the projectile had penetrated to a depth greater than its original diameter into the target, and had become severely distorted (Fig. 4). The plasticene clay lip above the original target surface grew substantially and is plotted specifically in Fig. 4 as a contour line marking a density of 1 Mg/m^3. The velocity vectors on the side of this contour in the direction of the target are generally moving uniformly radially outward from a point on-axis slightly behind the projectile. This region contained solid and some melted clay. The velocity vectors on the other side of the contour, inside the "hole" carved by the projectile and above the target surface, were moving in various directions, and the associated target material had a density much lower than 1 Mg/m^3 and was totally vaporized.

At 2.6 μsec the Lagrangian grid was discarded and the calculation continued using only the Eulerian grid, which then contained the aluminum projectile as well as the plasticene clay. The calculations were continued to a total time of 18 μsec in the present effort. The total calculated time seems very short; however, it must be kept in mind that these are simulations of laboratory-sized impacts. Using simple cube-root scaling of total energy and comparing the total calculated time scaled to the Johnie Boy nuclear explosive event yield (0.5 kt, or 2.0 TJ) gives 13 msec. As reported by Orphal (1977a), the early time coupling of the Johnie Boy nuclear device energy to the alluvium was complete by 7 msec, and

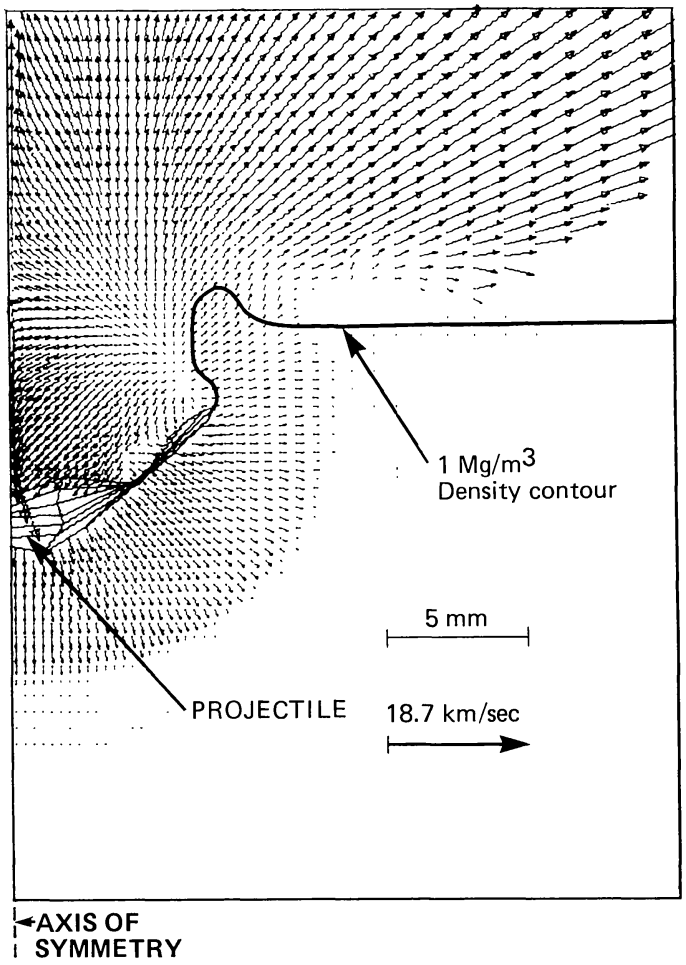

Fig. 4. Vector velocity plot in target material, and plot of projectile Lagrangian grid at 2.6 μsec (the high velocity target material above the 1 Mg/m^3 density contour is shock vaporized and $\rho \ll 1$ Mg/m^3).

the wall of the transient crater chosen at 7.84 msec. Thus our impact calculations had been carried to scaled times comparable to the early times of the Johnie Boy calculation.

MOMENTUM AND ENERGY TRANSFER TO THE TARGET

Treating the projectile at very early times in Lagrangian coordinates and using very small zones in the Eulerian target region allowed careful monitoring of the early energy and momentum transfer to the target as a function of penetration depth (the depth of that part of the projectile which had penetrated the deepest into the target) when the rate of transfer was the most rapid (Fig. 5). For reference, a plot of the projectile penetration depth vs. time is also given. With the projectile mass and impact velocity used in the calculations, momentum transfer to the target occurred at a slower rate than did energy transfer. At 18 μsec, the

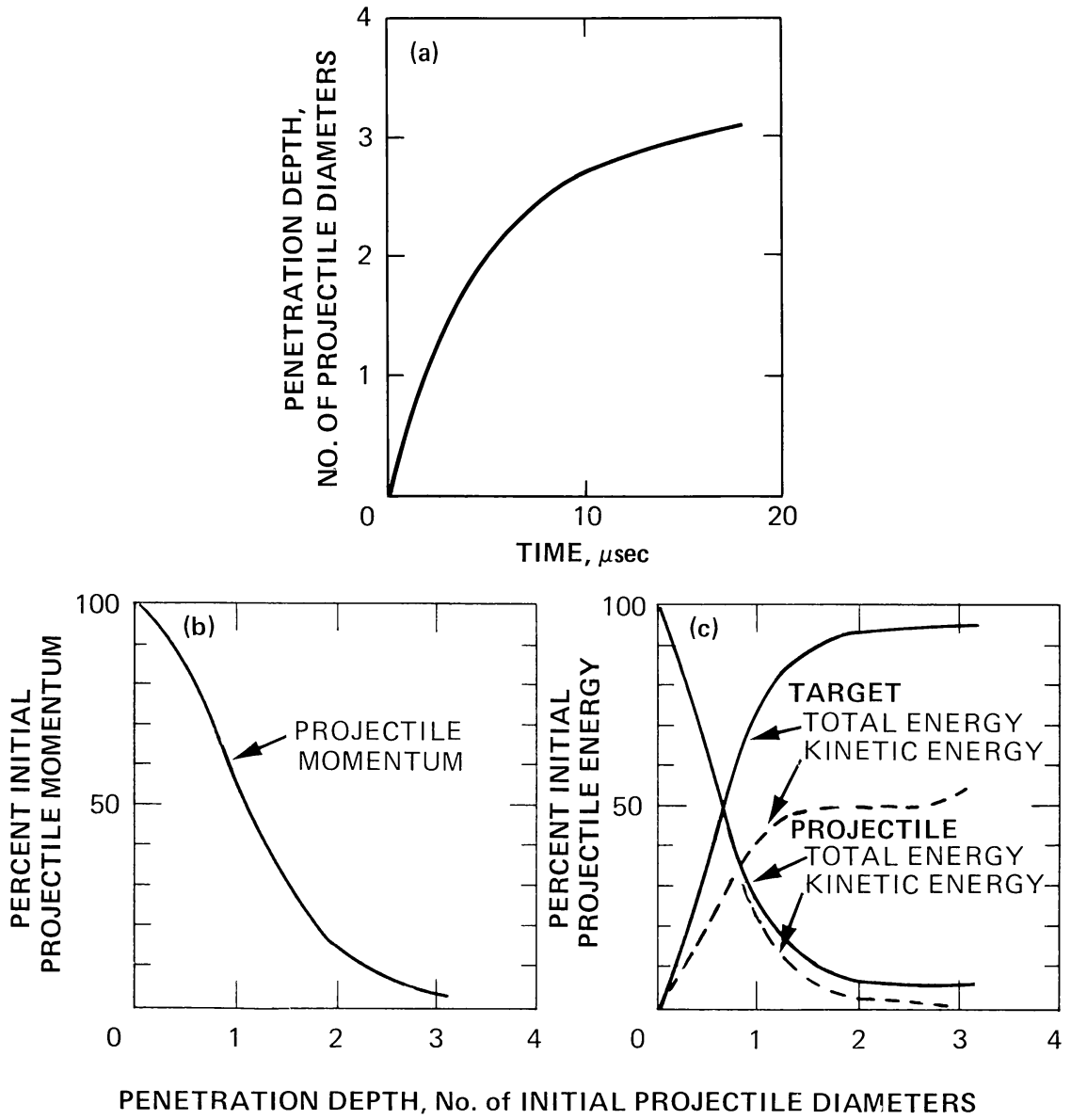

Fig. 5. Projectile penetration history (a) and momentum (b) and energy (c) transfer from the projectile to the target versus penetration depth.

projectile had penetrated to a depth of over 3 initial projectile diameters and no longer contained any appreciable kinetic energy. A small amount of momentum (~3 percent of the initial projectile momentum) was still retained by the projectile.

Although energy was rapidly coupled to the target, not all of it was available for excavation. Energy was absorbed through shock heating of the projectile (approximately 5 percent of the total impact energy, Fig. 5c), and more importantly through shock vaporization of the target material. The shock vaporized material escaped easily into the vacuum above the original target surface and no longer played a role in the excavation process.

At the approximate end of the compression stage of Gault *et al.* (1968), which occurs when the projectile penetrates the target to a depth equal to its original diameter, 70 percent of the total energy, but only 50 percent of the total momentum, had been transferred to the target. Thus, for the laboratory-scale impacts simulated by our calculations, the energy and momentum transfer process continues during the early part of the excavation stage.

The 1 Mg/m^3 density contour (e.g., Fig. 4) defined the wall of the transient crater because it was the best estimate of the boundary line between vaporized and non-vaporized target material. The kinetic energy coupled beyond this contour at later times (10 to 18 μsec) constituted 30 to 37 percent of the total impact energy. This was incorporated in the shock wave and in the region behind it and represented a maximum percentage of the initial impact energy available for excavation.

CRATERING FLOW FIELD ANALYSIS

The cratering flow field has been defined previously for explosion cratering (Orphal, 1977b) as the particle velocity flow field existing in the region of the transient crater but behind the initial out-going shock front (Fig. 6). Maxwell (1977) and Orphal (1977b) described an analytic model called Maxwell's Z-Model that was developed to describe the cratering motions observed in near-surface explosion cratering calculations. After the initial explosion, a shock wave propagates through the target material approximately spherically from the detonation point and decays rapidly. After the shock front passes, the shocked material retains a residual velocity which, subsequently modified by surface rarefactions and by

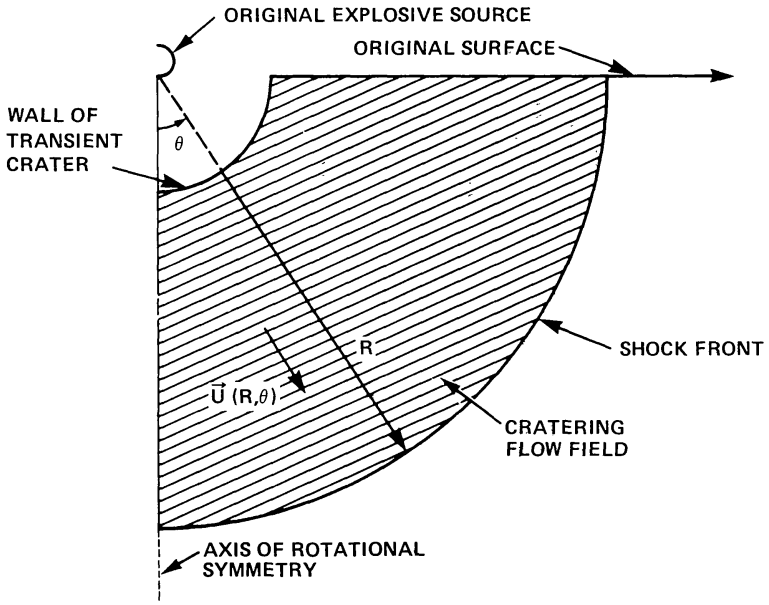

Fig. 6. This schematic representation shows the cratering flow field region as defined for near-surface explosion cratering calculations.

the effects of material strength and gravity, produces the final crater at much later times. Maxwell found for near-surface explosion calculations that at early times crater growth was nearly hemispherical. In spherical polar coordinates taken about the on-axis detonation point, the flow field could be described by

$$\dot{R} = \alpha(t)R^{-Z}, \tag{3}$$

where $\dot{R}$ is the radial velocity of the flow field, α is a time-dependent coupling term describing the flow field strength, and Z defines the rate of velocity decay with range, R. Maxwell (1977) also observed that the density in the cratering flow-field region was approximately constant, yielding incompressible flow:

$$\nabla \cdot U(R,\theta) = 0 \tag{4}$$

where $U(R,\theta)$ is the vector velocity of the flow field. Combining Equations 3 and 4 permits derivation of the full equation of motion of a mass element within the cratering flow field:

$$U(R,\theta) = \dot{R}\,\hat{R} + \dot{R}(Z - 2)\tan(\theta/2)\hat{\theta}, \tag{5}$$

where $\hat{R}$ and $\hat{\theta}$ are unit vectors in spherical polar coordinates. This can be integrated to give the mass element motion as a function of time. Gravity and material strength effects can also be included. It is clear from Equation 5 that for $Z = 2$, U is radial at all points, yielding an irrotational flow field. The corresponding physical case is the purely radial velocity field resulting from the explosion of a spherical source in an homogeneous medium of infinite extent in all directions. Maxwell (1977) found for near-surface explosion cratering calculations that $Z \approx 2$ for $\theta = 0°$, that $Z \approx 2.7$ for $30° \lesssim \theta \lesssim 60°$; and that $Z \gtrsim 4$ for $\theta \gtrsim 75°$. An average value of $Z \approx 3$ was found to be representative of the entire cratering flow field produced by a near-surface explosion. Values of $Z > 2$ lead to flow fields which are rotational in the direction of the surface (e.g., Orphal, 1977b). The rotation leads to the eventual ejection of material below the ground plane in a very orderly manner, beginning with material closest to the wall of the transient cavity. Total energy, material strength and gravity limit the total mass ejected, and also control the crater depth (e.g., O'Keefe and Ahrens, 1979).

We investigated the applicability of Maxwell's Z-Model to impact cratering, using our calculations simulating laboratory-scale impact. Because the impact cratering process is initially very different from the explosion cratering process, we felt it was particularly necessary to determine that Eq. 3 was valid. Figure 7a reveals that the wall of the transient crater at 18 μsec was nearly hemispherical about a point centered on-axis and 1.08 initial projectile diameters beneath the original target surface. In spherical polar coordinates taken about this point, the residual velocities within the cratering flow field were found to decay in the manner consistent with Eq. 3 (Fig. 7b). Secondary shocks behind the main shock front obscured the attenuation of $\dot{R}$ with R, and the actual calculation of α and Z was performed only in the region between the dotted lines ($15 \leq R \leq 23$ mm).

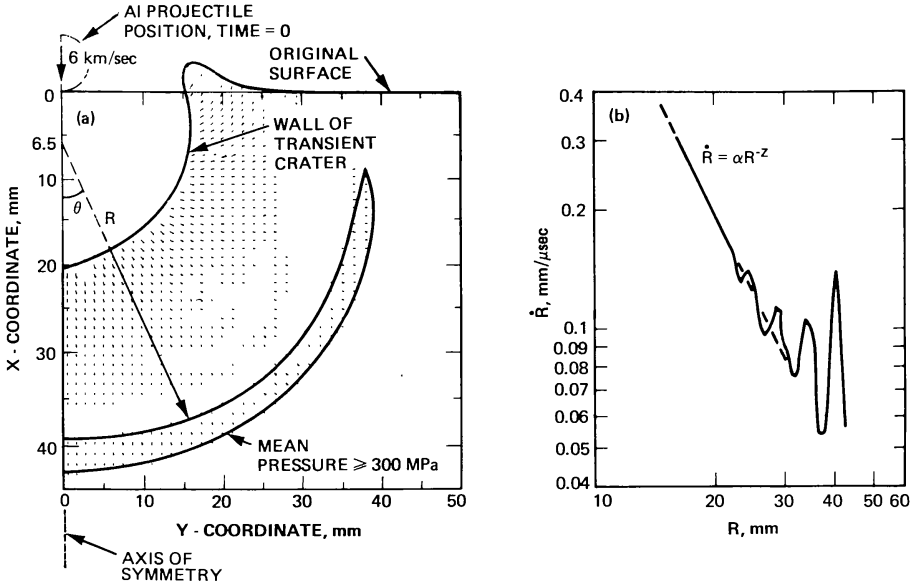

Fig. 7. Maxwell's Z-Model applied to a calculation of the impact of a 0.3 g aluminum projectile into a plasticene clay target at a velocity of 6 km/sec at a time of 18 μsec. a) Vector velocity plot in cratering flow field region, and spherical polar coordinates centered beneath the original target surface; b) Plot of $\dot{R}$ vs. R for $\theta = 30°$ with the values $\alpha = 76.0$ mm$^{Z+1}/\mu$sec and $Z = 2.017$ obtained from a fit to the calculated radial velocity field.

The computer routine developed to perform the cratering flow field Z-Model analysis calculated $\dot{R}$ and R about the flow center for 18 μsec at θ increments of 5°, and α and Z were plotted as a function of θ (Fig. 8). It is seen that α is nearly independent of θ in a manner similar to that observed in explosion calculations.

Various depths of the flow center were tried to determine if the true center was

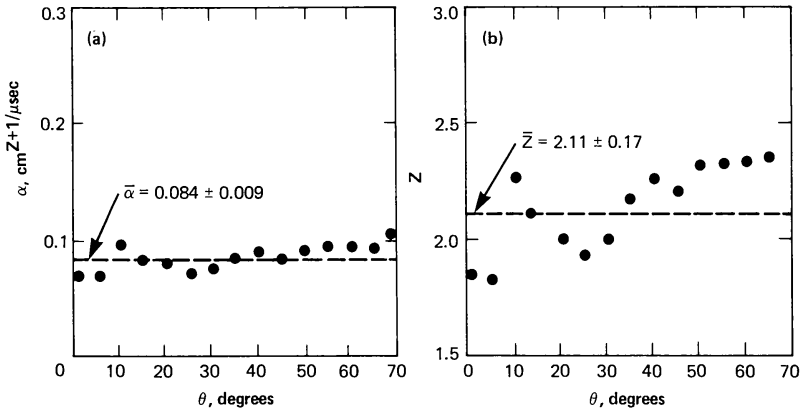

Fig. 8. These plots show the calculated values of α (a) and Z (b) versus θ for a flow field center taken at a depth of 6.5 mm at a time of 18 μsec. The values of α and Z were averaged over all values of θ and these values are shown as dotted lines on the respective plots. The standard deviations of $\bar{\alpha}$ and $\bar{Z}$ were also computed and are given in the plots.

indeed at a depth equal to 1.08 initial projectile diameters at 18 μsec. It was found that the chosen flow center first, minimized the standard deviation of α for $0 \leq \theta \leq 70°$; and secondly, gave the most regular variation of Z with θ. As expected, our calculation of low and higher strength targets gave identical results at this early time. Oberbeck (1971) found, for impact of aluminum projectiles into non-cohesive quartz sand targets at 2 km/sec, that the resulting crater was the same as an equivalent energy explosion-generated crater in the same material when the explosive was buried at a depth of 6.3 ± 2 mm beneath the target surface. In the framework of the Z-Model, this empirical result manifests itself in a cratering flow field centered below the target surface.

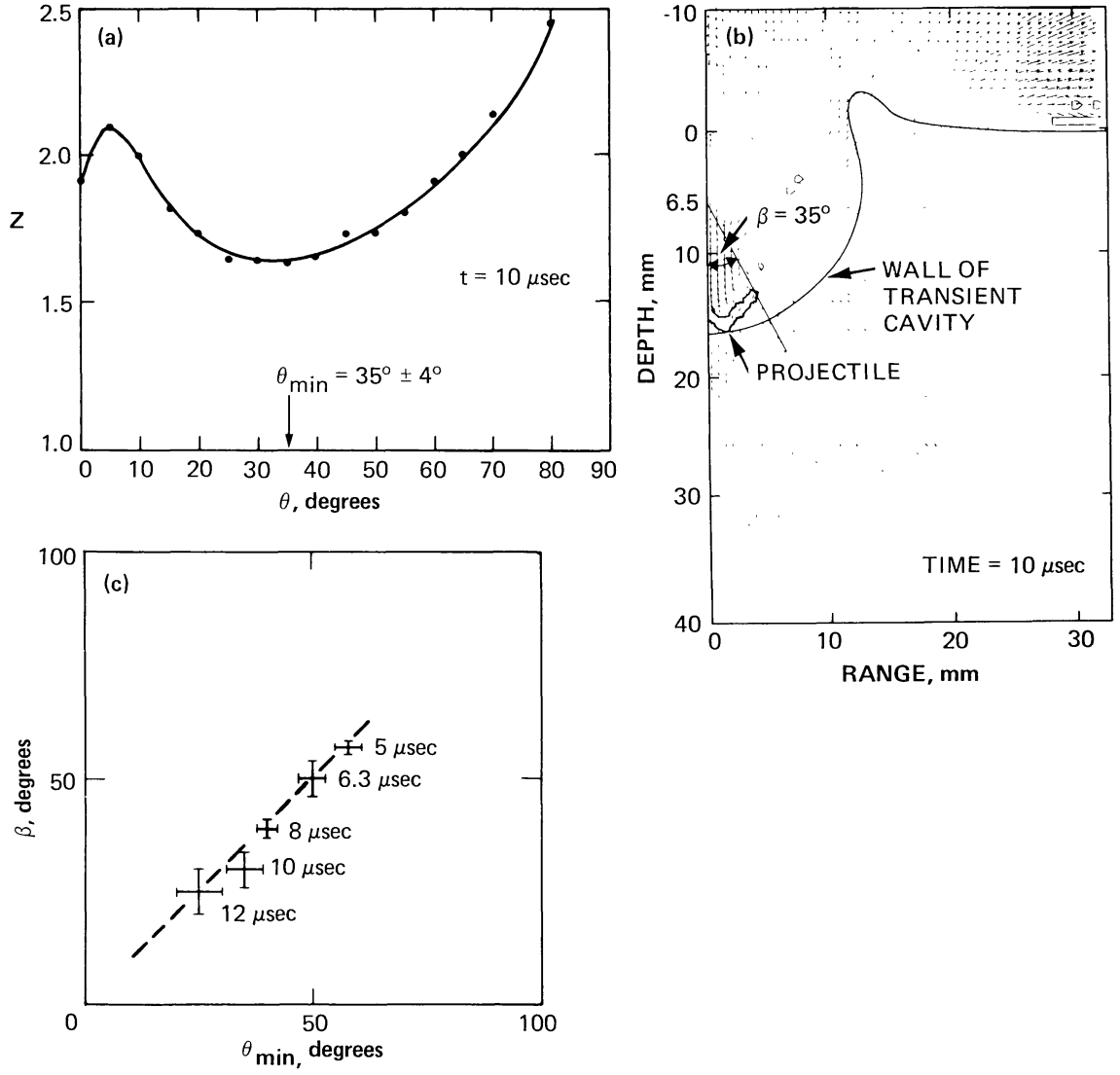

Fig. 9. These plots show the effect of the projectile on the early time Z flow field. a) A plot of Z vs. θ at t = 10 μsec shows values of $Z < 2$, with Z achieving a minimum at $\theta_{min} = 35°$. b) The angle subtended by the projectile (β) at 10 μsec is also about 35°. c) A plot of β vs. θ_{min} shows that a direct correlation holds during the early stages of the impact process.

For times less than about 12 μsec, the directed momentum of the projectile overdrove the cratering flow field in the target region beneath the projectile. This initial directedness of momentum (and kinetic energy) in an impact is a basic difference between an impact and an explosion event. Application of the Z-Model at these times using the 18 μsec flow field center yielded values of $Z < 2$ (Fig. 9a) over a considerable range of θ. A minimum value of Z was achieved for $\theta = \theta_{min}$ which we found to be directly correlatable with the maximum angle (β) subtended by the projectile from the flow field center (Fig. 9b). This correlation also held at earlier times (Fig. 9c) as long as the actual position of the projectile was below the flow center. Values of $Z < 2$ have not been seen in explosion cratering and the direct correlation of this effect with the projectile leads us to conclude that it is probably unique to impact cratering. By Equation 5 this leads to a flow field which is rotational in the downward direction, i.e., into the target. In this context, however, the effect is simply the manifestation of the almost completely expended projectile driving a continually more localized portion of the cratering flow field.

CONCLUSIONS

Major results from the two early time finite difference calculations of spherical aluminum projectile impact at 6 km/sec into homogeneous plasticene clay targets with differing von Mises material yield strengths are:

1. The magnitude of the target material jetting velocity which occurs upon projectile impact is in qualitative agreement with experimental observation.
2. The velocity field developed within the target is strikingly similar to those developed in near-surface explosion cratering calculations. This similarity has been quantified by extending Maxwell's Z-Model of explosion cratering to impact cratering.

Plasticene clay is a uniform material which is characterized by a simple material model and which is also readily available. Thus it is ideal for studies of basic cratering phenomenology employing either cratering calculations as in the present effort, or laboratory-scale experiments. It is probably not a good simulant of materials existing on lunar or planetary surfaces. Calculations were performed to an early time (18 μsec) for two von Mises strengths differing by a factor of 3; no differences in the computed results were seen and none were expected. At much later times during the cratering process, we do expect significant differences to develop, based on data from past laboratory-scale explosion cratering experiments.

We have carefully analyzed the impact-induced material motions, capturing first the initial jetting, then the deformation of the projectile and finally the response of the clay within the target. The major assumption of Maxwell's Z-Model (and the one which would not necessarily be valid for impact cratering), namely

the regular power law decay of $\dot{R}$ with R, was found to be valid at 18 μsec, provided that the center of the Z-Model coordinate system was chosen at a specific depth below the original target surface. This result differs from the surface-centered coordinate system employed in near-surface explosion cratering work, and is a consequence of the initial directedness of projectile momentum and kinetic energy. A second assumption, that of incompressible flow within the cratering flow field, will be tested as the calculations are continued; however, because the shock processes are the same in both explosion and impact events, we expect that this assumption will be valid.

The specific depth of the flow field center is suspected to depend strongly on the projectile material, and its initial energy and momentum. The projectile was not melted during the impact, but a significant amount of target material was vaporized in our calculations. For this case it was found that the center was located at a depth of 1.08 initial projectile diameters (6.5 mm) at 18 μsec. Further slight movement downward may occur as the calculations are continued. Calculational studies should be performed varying the projectile material and mass at constant initial kinetic energy to show explicitly the variation of the depth of the center with these quantities.

Acknowledgments—This work was supported by the National Aeronautics and Space Administration under Contract No. NASW-3168. We appreciate the critical review comments of J. Bryan and S. Croft on the manuscript. The Lunar and Planetary Institute is operated by the Universities Space Research Association under Contract No. NSR 09-051-001 with the National Aeronautics and Space Administration. This paper constitutes the Lunar and Planetary Institute Contribution No. 385.

REFERENCES

Bjork R. L. (1961) Analysis of the formation of Meteor Crater, Arizona: A preliminary report. *J. Geophys. Res.* **66,** 3379–3387.

Bryan J. B., Burton D. E., Cunningham M. E., and Lettis L. A. Jr. (1978) A two-dimensional computer simulation of hyper-velocity impact cratering: Some preliminary results for Meteor Crater, Arizona. *Proc. Lunar Planet. Sci. Conf. 9th,* p. 3931–3964.

Christensen D. M., Godfrey C. S., and Maxwell D. E. (1968) Calculations and model experiments to predict crater dimensions and free field motion. Report DASA-2360, Defense Atomic Support Agency, Washington, D.C. 78 pp.

Gault D. E. and Heitowit E. D. (1963) The partition of energy for hypervelocity impact craters formed in rock. *Proc. 6th Hypervelocity Impact Symposium,* p. 419–456. Clearinghouse for Federal Scientific and Technical Information.

Gault D. E., Quaide W. L., and Oberbeck V. R. (1968) Impact cratering mechanics and structures. In *Shock Metamorphism of Natural Materials* (B. M. French and N. M. Short, eds.), p. 87–99. Mono, Baltimore.

Gault D. E. and Wedekind J. A. (1977) Experimental hypervelocity impact into quartz sand—II effects of gravitational acceleration. In *Impact and Explosion Cratering* (D. J. Roddy, R. O. Pepin, and R. B. Merrill, eds.), p. 1231–1244. Pergamon, N.Y.

Gehring J. W. Jr. (1970) Theory of impact on thin targets and shields and correlation with experiment. In *High-Velocity Impact Phenomena* (R. Kinslow, ed.), p. 105–156. Academic, N.Y.

Hancock S. L. (1976) Finite difference equations for PISCES 2DELK, A coupled Euler Lagrange continuum mechanics computer program. Report TCAM 76-2. Physics International Company, San Leandro, Calif. 174 pp.

Holsapple K. A., and Schmidt R. M. (1979) A material strength model for apparent crater volume. *Proc. Lunar Planet. Sci. Conf. 10th*. This volume.

Maxwell D. E. (1977) Simple Z-model of cratering, ejection and the overturned flap. In *Impact and Explosion Cratering* (D. J. Roddy, R. O. Pepin, and R. B. Merrill, eds.), p. 1003–1008. Pergamon, N.Y.

Maxwell D. E., McKay M. W., Reaugh J. E., and Seifert K. D. (1972) Advanced methods to predict the response of a site under nuclear attack. Report PIPR 388-2. Physics International Company, San Leandro, Calif. 18 pp.

Maxwell D. E. and Reaugh J. E. (1972) Advanced methods to predict the response of a site under nuclear attack. Report PIPR-388-1, Physics International Company, San Leandro, Calif. 35 pp.

McQueen R. G., Marsh S. P., Taylor J. W., Fritz J. N., and Carter W. J. (1970). The equation of state of solids from shock wave studies. In *High-Velocity Impact Phenomena* (R. Kinslow, ed.), p. 293–417. Academic, N.Y.

Moore H. J. (1976) Missile impact craters (White Sands Missile Range, New Mexico) and applications to lunar research. *U.S. Geol. Survey Prof. Paper 812-B*. 47 pp.

Oberbeck V. R. (1971) Laboratory simulation of impact cratering with high explosives. *J. Geophys. Res.* **76,** 5732–5749.

O'Keefe J. D. and Ahrens T. J. (1975). Shock effects from a large impact on the moon. *Proc. Lunar Sci. Conf. 6th,* p. 2831–2844.

O'Keefe J. D. and Ahrens T. J. (1976) Impact ejecta on the moon. *Proc. Lunar Sci. Conf. 7th,* p. 3007–3025.

O'Keefe J. D. and Ahrens T. J. (1977) Impact-induced energy partitioning, melting, and vaporization on terrestrial planets. *Proc. Lunar Sci. Conf. 8th,* p. 3357–3374.

O'Keefe J. D. and Ahrens T. J. (1978) Impact flows and crater scaling on the moon. *Phys. Earth Planet. Inter.* **16,** 341–351.

O'Keefe J. D. and Ahrens T. J. (1979) The effect of gravity on impact crater excavation time and maximum depth; Comparison with experiment (abstract). In *Lunar and Planetary Science X,* p. 934–936. Lunar and Planetary Institute, Houston.

Orphal D. L. (1977a) Calculations of explosion cratering—I The shallow-buried nuclear detonation Johnie Boy. In *Impact and Explosion Cratering* (D. J. Roddy, R. O. Pepin, and R. B. Merrill, eds.), p. 897–906. Pergamon, N.Y.

Orphal D. L. (1977b) Calculations of explosion cratering—II Cratering mechanics and phenomenology. In *Impact and Explosion Cratering* (D. J. Roddy, R. O. Pepin, and R. B. Merrill, eds.), p. 907–917. Pergamon, N.Y.

van Thiel M. (1977) Compendium of shock wave data. Report UCRL 50108, Vol. 1. Lawrence Livermore Laboratory, Livermore, Calif. 331 pp.